Skp1 forms multiple protein complexes, including RAVE, a regulator of V-ATPase assembly

Jae Hong Seol*, Anna Shevchenko†, Andrej Shevchenko†‡ and Raymond J. Deshaies*§

*Division of Biology and Howard Hughes Medical Institute, California Institute of Technology, Pasadena, California 91125, USA
*†Protein and Peptide Group, European Molecular Biology Laboratory, Meyerhofstrasse 1, 69012 Heidelberg, Germany*
‡e-mail: shevchenko@embl-heidelberg.de
§e-mail: deshaies@its.caltech.edu

SCF ubiquitin ligases are composed of Skp1, Cdc53, Hrt1 and one member of a large family of substrate receptors known as F-box proteins (FBPs). Here we report the identification, using sequential rounds of epitope tagging, affinity purification and mass spectrometry, of 16 Skp1 and Cdc53-associated proteins in budding yeast, including all components of SCF, 9 FBPs, Yjr033 (Rav1) and Ydr202 (Rav2). Rav1, Rav2 and Skp1 form a complex that we have named 'regulator of the (H+)-ATPase of the vacuolar and endosomal membranes' (RAVE), which associates with the V_1 domain of the vacuolar membrane (H+)-ATPase (V-ATPase). V-ATPases are conserved throughout eukaryotes, and have been implicated in tumour metastasis and multidrug resistance, and here we show that RAVE promotes glucose-triggered assembly of the V-ATPase holoenzyme. Previous systematic genome-wide two-hybrid screens yielded 17 proteins that interact with Skp1 and Cdc53, only 3 of which overlap with those reported here. Thus, our results provide a distinct view of the interactions that link proteins into a comprehensive cellular network.

SCF ubiquitin ligases regulate a wide range of cellular processes, including immunity, signalling, cell division and transcription[1]. SCF contains four subunits — Skp1, Cdc53 (also known as cullin 1 or Cul1), an F-box protein, and the newly discovered

RING-H2 protein Hrt1 (also known as Roc1 or Rbx1; refs 2–5). A remarkable property of SCF ubiquitin ligases is that their specificity can be programmed through an array of distinct substrate receptors[6,7]. These receptors are recruited to SCF by the conserved F-box
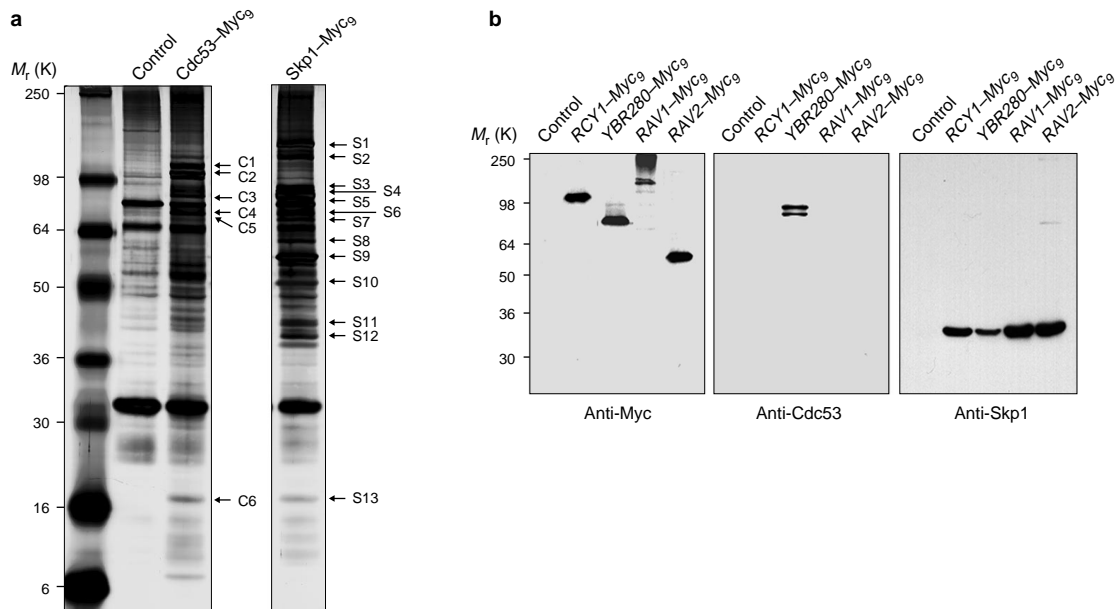
Figure 1 **Identification of proteins associated with Cdc53 and Skp1. a,** Proteins immunoprecipitated with an anti-Myc antibody (9E10) from 35 mg of wild-type, *CDC53–Myc9* and *SKP1–Myc9* cell extracts were eluted with SDS, separated in an 8–16% gradient SDS–polyacrylamide gel and visualized by silver staining. Specific bands present only in Cdc53–Myc9 or Skp1–Myc9 immunoprecipitates were identified by mass spectrometry. **b,** Extracts (6 mg) from untagged control, *RCY1–Myc9, YBR280–Myc9, RAV1–Myc9* and *RAV2–Myc9* cells were immunoprecipitated with 9E10, fractionated by SDS–PAGE, and immunoblotted with antibodies against Myc, Cdc53 or Skp1 as indicated.

Table 1 Cdc53-and Skp1-associated proteins indentified by SEAM

Identification	ORF	Comments	ORF	Comments	ORF	Comments
Cdc53 interactors*						
C3	Ylr352	F-box[†]	Ylr352[‡]		Ylr100	Erg27
C4	Yjl149[§]	F-box[†¶]			Ylr128	
C5	Yml088	F-box[†]			Ydr328	Skp1
C6	Yol1033[§]	Hrt1			Ylr368	F-box
					Ygl249	Zip2
					Ydl017	Cdc7
Skp1 interactors*						
S1	Yjr033	Rav1			Ylr399	Bdf1
S2			Yjr090	Grr1[†¶#]		
S3	Ydr385	EF-2**			Yfl009	Cdc4
S4	Yjl204[§]	Rcy1[†¶#]			Ymr094	Ctf13[††]
S5	Ydl132	Cdc53			Yil046	Met30
S6	Yjl149[§]	F-box[†¶]			Ydr139	Rub1
S7	Ybr280	F-box[†¶]			Yor057	Sgt1
S8	Ymr168	Cep3[††]			Ylr224	F-box
S9	Ymr258	F-box[†¶]	Ylr352[‡]		Ylr352	F-box
S11			Ylr097	F-box[†¶]		
S12	Ydr202	Rav2			Ylr368	F-box
S13	Yol133[§]	Hrt1				

← SEAM →	← Overlap →	← Two-hybrid screen →

ORF, open reading frame.
*C1 (modified with Rub1) and C2 are Cdc53; S10 is Skp1.
F-box proteins, as confirmed by [†]sequence homology, [¶]co-immunoprecipitation with Skp1, and [#]functional studies.
[‡]Ylr352 was identified as a Cdc53 interactor by affinity purification and protein sequencing, and as a Skp1 interactor by genome-wide two-hybrid analysis.
[§]Yjl149, Yjl204 and Yol133 baits were used in genome-wide two-hybrid screens, but no specific interacting proteins were consistently identified.
**EF-2 binds strongly to the abundant F-box protein Ylr097 (A. Shevchenko & M. Tyers, personal communication).
[††]Cep3 and Ctf13 are both subunits, along with Skp1, of the CBF3 complex.

domain, and are tethered to the Cdc53/Hrt1 ubiquitin-ligase module by Skp1. The genome of budding yeast encodes 16 proteins that contain an obvious F-box motif[7], and at least 3 of these proteins assemble into SCF complexes *in vivo*[8]. Despite rapid advances in our understanding of the structure and activity of SCF, very little is known about how this family of ubiquitin ligases is integrated into cell physiology in a global sense.

A common strategy for deducing the physiological transactions of proteins is to look for interacting partners. Considerable effort has already been invested in sequential or massively parallel genome-wide two-hybrid screens for interacting proteins[9,10]. However, in two-hybrid screens, interacting proteins are detected in a pair-wise manner, which is a significant limitation, as many of the proteins that are involved in cell duplication are assembled into multisubunit complexes (such as SCF, the origin-recognition complex and the anaphase-promoting complex (APC). Protein–protein interactions within or between protein complexes may not be detected in two-hybrid screens if either the bait or the prey fails to assemble properly with other subunits of the complex.

As an alternative method to map out a network of protein interactions, we used affinity purification followed by mass spectrometry. In this approach, candidate genes are tagged with a sequence encoding an epitope that is recognized by monoclonal antibodies, and the epitope-tagged protein, together with any associated polypeptides, is recovered by immunoprecipitation from a whole-cell lysate. Proteins that interact with the tagged subunit are separated by gel electrophoresis and then identified by mass spectrometry. New proteins identified in this manner are then tagged, and the entire process is repeated. By sequential rounds of epitope tagging, affinity purification and mass spectrometry (the entire process being termed SEAM), a network of interacting proteins can be revealed. In contrast to two-hybrid methods, this approach can identify entire protein complexes, as well as interactions between distinct complexes, in a single step.

Here we report the use of SEAM to identify a new Skp1-containing complex, RAVE, which associates with the V_1 domain of the V-ATPase. V-ATPase is an ATP-dependent proton pump that functions in both intracellular membranes and, in certain cell types, the plasma membrane[11]. V-ATPase within intracellular compartments functions in processes such as receptor-mediated endocytosis, intracellular targeting of lysosomal enzymes, protein processing and degradation, viral entry, and coupled transport of small molecules, such as neurotransmitters[11]. On the other hand, V-ATPase within the plasma membrane is involved in bone resorption, renal acidification, pH homeostasis and K^+ secretion[11]. The V-ATPase holoenzyme is composed of two distinct protein complexes, V_0 and V_1. The V_0 complex, which is embedded in the vacuolar membrane, contains five subunits and forms a proton channel, whereas the V_1 complex, which docks to the cytosolic surface of the V_0 complex, comprises eight subunits and contains the active sites for ATP
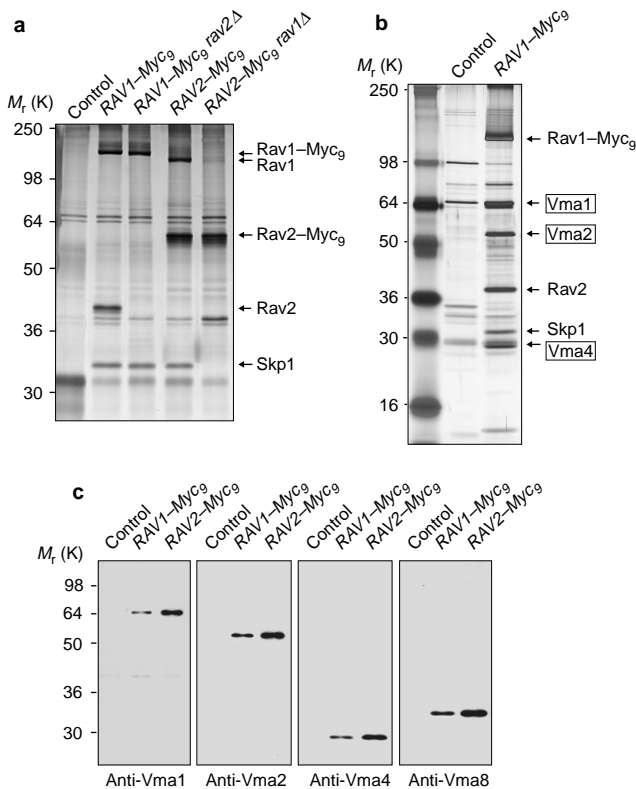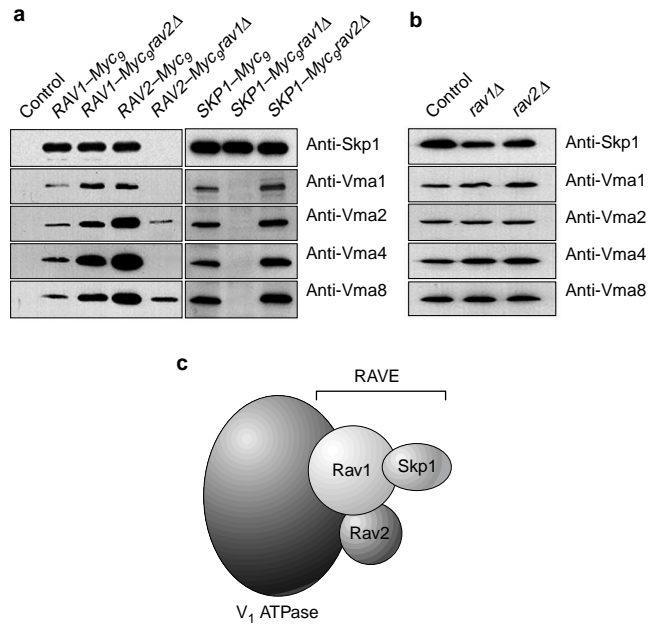
Figure 2 **Rav1, Rav2 and Skp1 form RAVE, which binds to V-ATPase. a,** Interaction between Rav1, Rav2 and Skp1. Extracts (6 mg) from untagged control, *RAV1–Myc9*, *RAV2–Myc9*, *RAV1–Myc9 rav2Δ* and *RAV2–Myc9 rav1Δ* cells were immunoprecipitated with anti-Myc antibody (9E10) in the presence of 0.5% Triton X-100, separated by SDS–PAGE, and stained with silver. **b,** Isolation of Rav1-associated proteins. Extracts (35 mg) of wild-type and *RAV1–Myc9* cells were processed as described in Fig. 1a, except that the immunoprecipitation buffer contained 0.2% Triton X-100, and 9E10 beads were eluted with tobacco etch virus protease. Rav2, Skp1 and subunits of V-ATPase (Vma1, Vma2 and Vma4) were identified as Rav1-interacting proteins by mass spectrometry. **c,** V-ATPase subunits interact specifically with Rav1 and Rav2. Proteins from lysates (6 mg) of untagged control, *RAV1–Myc9* and *RAV2–Myc9* cells were immunoprecipitated with 9E10, fractionated by SDS–PAGE, and immunoblotted with antibodies against the V-ATPase subunits Vma1, Vma2, Vma4 and Vma8, as indicated.

Figure 3 **Topology of the RAVE complex. a,** Skp1 is linked to V-ATPase through Rav1. Proteins from untagged control, *RAV1–Myc9*, *RAV2–Myc9*, *RAV1–Myc9 rav2Δ*, *RAV2–Myc9 rav1Δ*, *SKP1–Myc9*, *SKP1–Myc9 rav1Δ* and *SKP1–Myc9 rav2Δ* cells were immunoprecipitated with anti-Myc antibody (9E10), separated by SDS–PAGE and immunoblotted with antibodies against Vma or Skp1, as indicated. **b,** Accumulation of Vma subunits in *rav1Δ* and *rav2Δ* mutants. Extracts (15 μg) from wild-type, *rav1Δ* and *rav2Δ* cells were separated by SDS–PAGE and immunoblotted with anti-Vma antibodies. **c.** Schematic diagram showing the organization of subunits within RAVE and the RAVE–V1 supercomplex.

hydrolysis[11,12]. After the V_0–V_1 ATPase is assembled, its activity can be regulated post-translationally; for example, in cells deprived of glucose, V_1 abruptly and reversibly detaches from V_0 (ref.13). Proper regulation of V_0–V_1 activity is likely to be crucial for cell physiology, as the proton gradient across the vacuolar membrane drives the uptake of a variety of metabolites into the vacuole. This idea is supported by the fact that thermal inactivation of the Vma4 subunit of budding yeast V-ATPase evokes transient defects in actin polarization, bud morphogenesis and cytokinesis[14]. Despite the importance of V-ATPase activity for cellular homeostasis, the molecular mechanisms by which this enzyme is regulated have remained elusive.

Results

Identification of proteins associated with Cdc53 and Skp1. To gain insight into how the potentially diverse array of SCF complexes and their component subunits are integrated into the regulatory fabric of the cell, we sought to identify proteins that associate with SCF subunits *in vivo*. We constructed versions of Cdc53 and Skp1 each fused to nine copies of the Myc epitope at their C termini (Cdc53–Myc9 and Skp1–Myc9) using a tagging method based on the polymerase chain reaction (PCR)[5]. Affinity purification using an anti-Myc monoclonal antibody (9E10) showed that many specifically co-precipitating polypeptides were recovered from tagged strains (Fig. 1a). Identification of these bands by mass spectrometry revealed the presence of 15 different proteins — Cdc53, Skp1, Hrt1, 7 FBPs (including previously unrecognized FBPs Ybr280 and Ymr258), a subunit of the Skp1-containing CBF3 complex, and the uncharacterized proteins Yjr033 and Ydr202 (Table 1). On the basis of the results presented below, we have renamed Yjr033 and Ydr202 as Rav1 and Rav2, respectively.

To investigate the physiological functions of these proteins, we first disrupted the corresponding genes. This analysis revealed that *hrt1Δ* strains were inviable[5], whereas *rav1Δ*, *yjl204Δ* (since renamed *rcy1Δ*; ref. 15) and *ybr280Δ* strains grew more slowly than the wild type, and *rav2Δ* cells exhibited no obvious phenotype. To confirm that the proteins encoded by these genes interact with Skp1, and to test for their potential incorporation into SCF complexes, we modified the corresponding chromosomal loci to encode proteins that were tagged with the Myc9 epitope. We immunoprecipitated extracts from *RCY1–Myc9*, *YBR280–Myc9*, *RAV1–Myc9* and *RAV2–Myc9* cells with anti-Myc beads, and immunoblotted them with antibodies against Cdc53 and Skp1. Whereas Skp1 co-immunoprecipitated with all four proteins, only Ybr280 associated with Cdc53 (Fig. 1b). These results indicate that the previously unrecognized F-box motif in Ybr280 may recruit this protein into an SCF complex. The absence of Cdc53 from Rcy1–Skp1 complexes is inconsistent with the idea that Skp1 is sufficient to link FBPs to cullins, and implies that FBPs contribute to the assembly of Cdc53 into SCF complexes.

386

NATURE CELL BIOLOGY | VOL 3 | APRIL 2001 | http://cellbio.nature.com
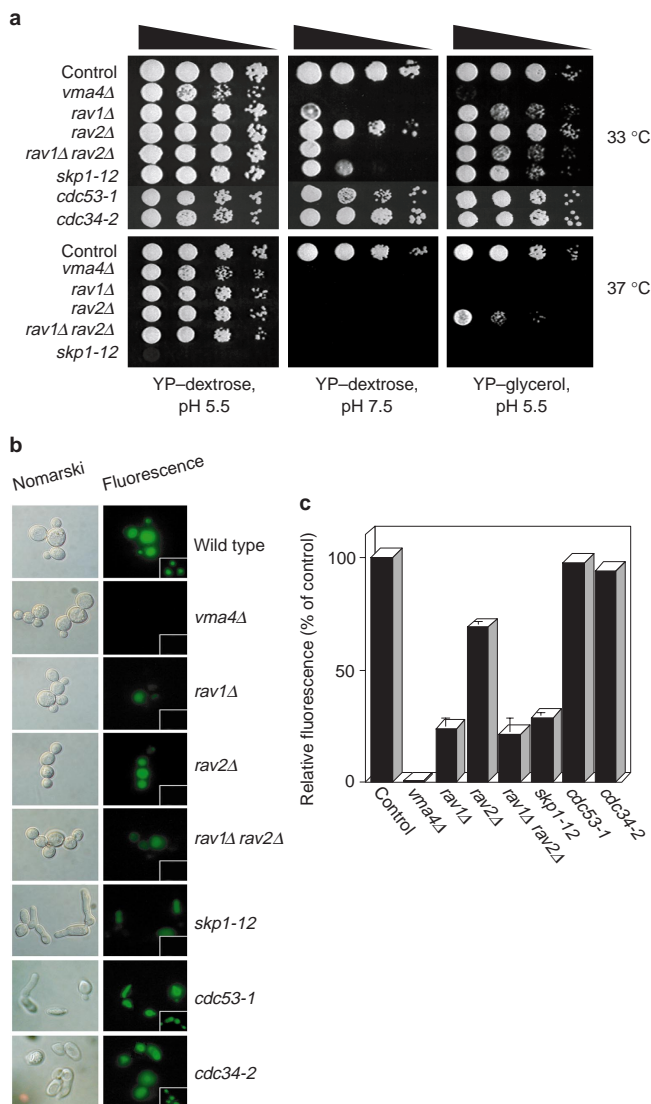
Figure 4 **RAVE mutants exhibit V-ATPase deficiency. a**, Tenfold serial dilutions of cells of the indicated strains grown on YP–dextrose (pH 5.5) were spotted onto YP–dextrose (pH 5.5 or 7.5) or YP–glycerol (pH 5.5) plates and grown for 3 days at the indicated temperature. **b**, **c**, Vacuolar labelling with quinacrine. Vacuolar acidification was monitored by accumulation of the fluorescent dye quinacrine within the vacuole. Cells grown on YP–dextrose (pH 5.5) at 33 °C (or pre-incubated at 37 °C for 1 h; see insets **b**) were transferred to uptake buffer (YP–dextrose, pH 7.5) and stained with 200 µM quinacrine. Dye uptake was monitored by microscopic examination of single cells (**b**) and by spectrofluorometric analysis of populations of cells (**c**; see Methods). Data in **c** are means ± s.d. (n = 3).

Rav1, Rav2 and Skp1 form RAVE, which binds to V-ATPase. Genome-wide systematic gene deletion[16], messenger RNA expression profiling[17], and two-hybrid[18] and bioinformatic[19] analyses have all failed to identify a clear function of Rav1 or Rav2. Therefore, to investigate the cellular functions of these proteins, we modified chromosomal *RAV1* and *RAV2* to encode Myc$_9$-tagged proteins, and then isolated the interacting partners by immunoaffinity chromatography and identified them by mass spectrometry as described above. Examination of proteins that co-immunoprecipitated with Rav1–Myc$_9$ under stringent washing conditions (0.5% Triton X-100) revealed the presence of Rav2 and Skp1 (Fig. 2a), indicating that these three polypeptides may form a new protein

complex. In co-immunoprecipitation experiments using mutant strains, Rav1 (but not Rav2) bound directly to Skp1 (Fig. 2a), despite possessing neither an F-box motif nor homology to the amino-terminal Skp1-binding domain of Cul1. We propose that Skp1–Rav1–Rav2, like CBF3 (ref. 20) and Rcy1–Skp1 (ref. 21) form a new Skp1-containing complex that does not function as an ubiquitin ligase.

To identify more loosely bound targets or regulators of the Skp1–Rav1–Rav2 complex, we repeated the affinity purification of Rav1–Myc$_9$ under low-stringency conditions (0.2% Triton X-100). Analysis of the resulting immunoprecipitate by mass spectrometry (Fig. 2b) revealed the presence of Skp1, Rav1, and Rav2, as well as three subunits of the V-ATPase (Vma1, Vma2 and Vma4). To reflect the functional relationship between Skp1–Rav1–Rav2 and V-ATPase (see below), we have named the complex 'regulator of the (H$^+$)-ATPase of the vacuolar and endosomal membranes (RAVE).
Topology of the RAVE complex. Immunoblotting experiments confirmed that Vma1, Vma2, Vma4 and also Vma8 were specifically associated with both Rav1–Myc$_9$ and Rav2–Myc$_9$ (Fig. 2c). To investigate the topology of the interaction between RAVE and the V$_1$ subunit of V-ATPase, we carried out co-immunoprecipitation experiments using *rav1Δ* and *rav2Δ* strains. Whereas RAVE subunits co-immunoprecipitated varying amounts of V$_1$ from wild-type cells, Skp1–Myc$_9$ failed to associate with V$_1$ in *rav1Δ* cells (Fig. 3a). In addition, Skp1, Vma1 and Vma4 were absent and only small amounts of Vma2 and Vma8 were recovered in anti-Myc immunoprecipitates prepared using *RAV2–Myc$_9$ rav1Δ* cells. Control immunoblots confirmed that levels of Vma subunits were unaffected in *rav1Δ* and *rav2Δ* cells (Fig. 3b). Together, these results indicate that Rav1 may bind directly to V$_1$, and may in turn link this subunit to both Skp1 and Rav2 (Fig. 3c).
RAVE mutants exhibit V-ATPase deficiency. To evaluate a possible function of RAVE in V-ATPase function, we investigated the growth phenotypes of *rav1Δ, rav2Δ, rav1Δ rav2Δ, skp1-12, cdc53-1* and *cdc34-2* cells under various conditions. All mutants had growth rates that were roughly similar to that of the wild type on YP–dextrose (pH 5.5; see methods) at 33 °C and 37 °C (Fig. 4a; we did not evaluate *skp1-12*, *cdc53-1* and *cdc34-2* strains at 37 °C because these mutants are temperature-sensitive for growth). Consistent with a previous report[22], cells lacking the Vma4 subunit of V$_1$ were unable to grow on YP–dextrose (pH 7.5) or YP–glycerol (pH 5.5), at either 33 °C or 37 °C. At 33 °C, *rav1Δ* and *skp1-12* cells exhibited a substantial reduction in growth on YP–dextrose (pH 7.5) and YP–glycerol (pH 5.5), and *rav1Δ* cells were unable to grow on these media at 37 °C. Although *rav2Δ* cells exhibited similar defects to *rav1Δ* and *skp1-12* mutants, their phenotypes were milder and were strikingly evident only at 37 °C. On the other hand, the growth phenotypes of the SCF-pathway mutants *cdc53-1* and *cdc34-2* were similar to the wild type at 33 °C on all media.

We explored further the functional relationship between RAVE and V-ATPase by monitoring V-ATPase-dependent vacuolar acidification in wild-type and mutant cells. We collected cells grown on YP–dextrose (pH 5.5) at 33 °C, washed them with YP–dextrose (pH 7.5), and incubated them with quinacrine, a weakly basic dye that accumulates in low-pH compartments[23]. Mutant *vma4Δ* cells failed to accumulate quinacrine, and *rav1Δ, rav2Δ, rav1Δ rav2Δ* and *skp1-12* cells exhibited a reduction in dye uptake (Fig. 4b, c) that paralleled the effect of these mutations on cell growth in buffered medium (Fig. 4a). The diminution of dye uptake observed at 33 °C was exacerbated further at higher temperatures — at 37 °C on YP–dextrose (pH 7.5), the quinacrine-uptake defects of *rav1Δ, rav2Δ* and *skp1-12* strains were as severe as that exhibited by *vma4Δ* cells (Fig. 4b, see insets). In contrast, *cdc53-1* and *cdc34-2* cells showed the same extent of dye uptake as the wild type at both 33 °C and 37 °C. Together, these results indicate that RAVE (but not SCF) may positively regulate V-ATPase activity *in vivo*.
Cytoplasmic RAVE promotes glucose-regulated assembly of V$_1$ with V$_0$ to form V-ATPase holoenzyme. What is the mechanism of

 387
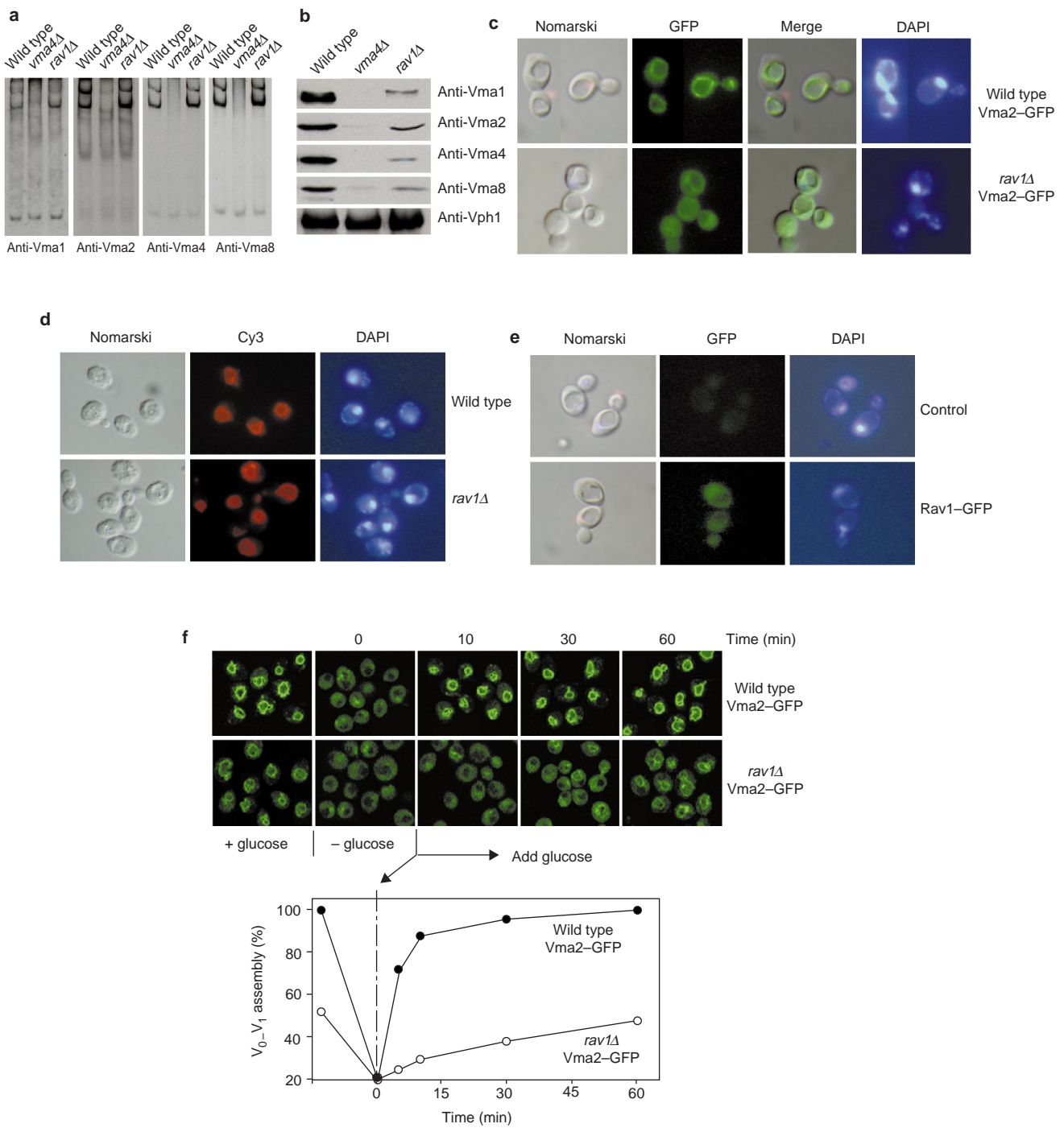
Figure 5 Cytoplasmic RAVE promotes glucose-regulated assembly of V$_1$ with V$_0$ to form the V-ATPase holoenzyme. a, b, To analyse the formation of V$_1$ and assembly of V$_0$–V$_1$ holoenzyme in wild-type, *vma4Δ* and *rav1Δ* strains, cells were grown at 33 °C in YP–dextrose (pH 5.5) and then transferred to YP–dextrose (pH 7.5) for 1 h at 33 °C before analysis. **a,** Effects of the *rav1Δ* mutation on formation of intact V$_1$. Soluble proteins (20 μg) from the indicated strains were fractionated in 6% acrylamide gel under native conditions, and immunoblotted with the indicated anti-Vma antibodies. **b,** Effect of the *rav1Δ* mutation on docking of V$_1$ to V$_0$. Crude membranes (10 μg protein) from the indicated strains were separated by SDS–PAGE and immunoblotted with antibodies against Vph1 or the indicated Vma subunits. **c–e,** *In vivo* localization of V$_1$ (**c**), V$_0$ (**d**) and RAVE (**e**). Localizations of Vma2–GFP and Rav1–GFP in live cells were examined by fluorescence microscopy. Both constructs were integrated at their respective chromosomal loci and were expressed from their natural promoters. Vph1, a subunit of V$_0$, was immunolocalized by indirect immunofluorescence (see Methods). Merged images in **c** are overlays of Nomarski and GFP images. DNA was visualized by staining with DAPI. **f,** Kinetics of assembly of V-ATPase in wild-type and *rav1Δ* cells. Wild-type and *rav1Δ* cells expressing Vma2–GFP were grown at 25 °C on YP–dextrose (pH 5.5) and then shifted to YP (pH 5.5) media. After glucose depletion for 10 min, cells were supplemented with 2% glucose to initiate V-ATPase reassembly and then re-incubated at 25 °C for the indicated times. Cells were then fixed and examined by confocal microscopy (upper panel). Relative V$_0$–V$_1$ assembly (expressed as vacuolar membrane staining intensity divided by cytoplasmic staining intensity for Vma2–GFP) was quantified (lower panel) by evaluation of the digital files using NIH image software. The amount of assembled V-ATPase in wild-type cells in the presence of glucose is designated as 100%.
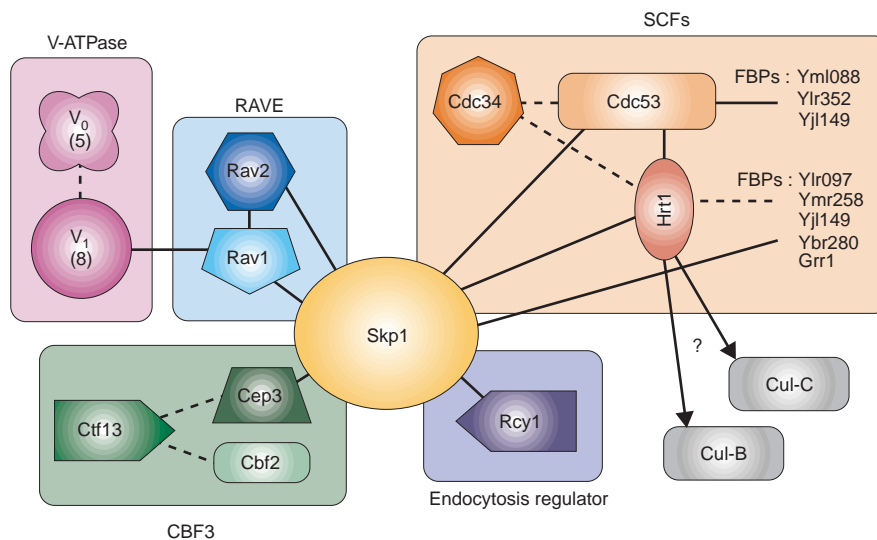
Figure 6 **Network of protein interactions involving Cdc53 and Skp1**. Solid lines indicate protein–protein interactions identified here; these interactions are not necessarily direct. Dashed lines refer to protein interactions that have been described elsewhere. Arrows refer to proposed interactions that have not yet been reported. Individual complexes within the network are indicated (V-ATPase, RAVE, SCFs, CBF3 and Rcy1–Skp1). Further links in the network are likely to exist, on the basis of the results of genome-wide two-hybrid screens[10].

action of the RAVE complex? Because *rav1Δ* and *rav2Δ* cells contained Vma subunits (Fig. 3b), but nevertheless exhibited a defect in V-ATPase-dependent vacuolar acidification, we hypothesized that RAVE promotes accumulation of the intact V_1 domain, assembly/transport of the intact V_0 domain, or formation of V_0–V_1 holoenzyme. To distinguish between these possibilities, we investigated V_1 and V_0 formation in *rav1Δ* cells using non-denaturing gel electrophoresis and immunofluorescence microscopy, respectively. V_1 domains were absent in *vma4Δ* cells (Fig. 5a) but accumulated normally in *rav1Δ* cells at permissive temperature (data not shown) or upon shift to conditions that did not allow growth (1 h in YP–dextrose (pH 7.5) at 33 °C; Fig. 4a), which is inconsistent with the idea that RAVE functions in formation or maintenance of intact V_1 complexes. Likewise, the V_0 subunit Vph1 was properly localized to the vacuolar membrane in *rav1Δ* cells at 37 °C (Fig. 5d). Vacuolar delivery of Vph1 serves as a surrogate marker for proper V_0 assembly[11,24].

Next, to determine the effects of RAVE on assembly of V_0–V_1 holoenzyme, we isolated a crude membrane fraction containing vacuolar membranes, from wild-type, *vma4Δ* and *rav1Δ* cells that were shifted to nonpermissive conditions (Fig. 5b). Immunoblotting revealed that membranes from wild-type cells contained high levels of Vma1, 2, 4 and 8. In contrast, Vma subunits were not detected in membranes from *vma4Δ* cells, and were present at greatly reduced levels in *rav1Δ* preparations. The Vph1 subunit of V_0 was present in equivalent amounts in all preparations, showing that the experiment was properly controlled. Similar results were obtained using cells grown under 'permissive' conditions (25 °C; data not shown). These observations thus implicate RAVE in docking of V_1 with membrane-embedded V_0. To investigate the function of RAVE in stable accumulation of V_0–V_1 holoenzyme *in vivo*, we constructed wild-type and *rav1Δ* strains that expressed green fluorescent protein fused to Vma2 (Vma2–GFP). We evaluated cells shifted to nonpermissive conditions as described above for Vma2–GFP fluorescence. The V_1 complex decorated the vacuolar membrane in wild-type cells, but was delocalized throughout the cytoplasm in *rav1Δ* cells (Fig. 5c).

Our analysis so far was consistent with the idea that RAVE serves either to stabilize assembled V_0–V_1 complexes or as an assembly

factor to promote binding of V_1 to V_0. To dissect further the mechanism of action of RAVE, we carried out an *in vivo* pulse–chase assembly experiment. Intact V_0–V_1 holoenzyme is rapidly disassembled in cells that are deprived of glucose[13]. We therefore cultured wild-type and *rav1Δ* cells expressing Vma2–GFP at 25 °C, shifted them to glucose-depleted medium for 10 min to promote detachment of V_1 from V_0, and then re-supplemented them with glucose. Glucose signalling promoted recruitment of V_1 to the vacuolar membrane within 10 min in wild-type cells (Fig. 5f). In contrast, reassembly of V-ATPase in *rav1Δ* cells proceeded much more slowly, but eventually recovered to the original state. Steady-state assembly of V_0–V_1 in *rav1Δ* cells was ~50% less than in wild-type cells under permissive conditions. Thus, in *rav1Δ* cells, formation of holoenzyme proceeded slowly at 25 °C (Fig. 5f), and was essentially blocked at high temperature (Fig. 5c). The hypothesis that RAVE acts transiently to catalyse assembly of cytoplasmic V_1 with membrane-embedded V_0 is supported by the observations that RAVE was associated with V_1 domains but not with intact V_1–V_0 holoenzyme upon conventional purification (P. Kane, personal communication), and that Rav1–GFP localized throughout the cytoplasmic compartment but did not label the vacuolar membrane (Fig. 5e).

Discussion

We have used iterative rounds of affinity purification and mass spectrometry to decipher a network of interacting proteins anchored by the core SCF subunit Skp1 (Fig. 6). Our approach identified sixteen SCF-associated polypeptides, which comprise at least seven distinct Skp1-containing complexes, including three (RAVE, Cep3–Skp1 (ref. 20) and Rcy1–Skp1) that lack Cdc53 and are likely to have functions other than ubiquitination, two SCF complexes (containing FBPs Ybr280 and Grr1), and two uncharacterized complexes (containing FBPs Yjl149 and Yml088). We have therefore shown that Skp1 forms multiple complexes (with and without FBPs) with diverse biochemical activities, and have thus provided new insight into the biological functions of Skp1 at the junction of several intracellular regulatory pathways.

Because of its generic and rapid nature, our approach provides an alternative to sequential two-hybrid screening[10] as a tool for

proteome exploration. Combining rapid epitope-tagging and two-step affinity purification[25] with automated single-step analysis of unfractionated immunoprecipitates by mass spectrometry[26,27] may provide a useful complement to genome-wide two-hybrid screens[18] as a means by which to deduce the entire set of protein complexes in a eukaryotic cell. Interestingly, comparison of Skp1- and Cdc53-interacting proteins identified by systematic two-hybrid screens[18] with those identified using the approach described here reveals that although each method uncovered ~15 interacting proteins, there is surprisingly little overlap between the two sets (Table 1). This underlines the fact that it is essential to use multiple methods to deduce the structure of eukaryotic proteomes.

We have established that Skp1, Rav1 and Rav2 associate to form RAVE, which promotes V-ATPase activity by stimulating assembly of V_1–V_0. Although V-ATPase-deficient cells grow normally on buffered medium, rapid thermal inactivation of V-ATPase elicits a range of cellular defects, including formation of abnormal buds and delocalization of both actin and chitin[14]. Moreover, V-ATPase is rapidly and reversibly inactivated by dissociation of V_1 from V_0 upon glucose deprivation, indicating that dynamic control of V-ATPase assembly may be intimately linked to cell physiology[13]. Glucose seems to govern V-ATPase assembly by a regulatory pathway that remains to be identified[13]. Because RAVE is required for rapid reassembly of V-ATPase upon addition of glucose to starved cells (Fig. 5f), it is possible that modulation of the activity of RAVE (or of a protein that is recruited to V_1 by RAVE) by a glycolytic metabolite links extracellular glucose concentration to the assembly state of V-ATPase.

RAVE clearly increases the rate at which V-ATPase holoenzyme complexes accumulate upon addition of glucose to starved cells (Fig. 5f). However, RAVE also seems to stabilize assembled V-ATPase. The steady-state level of Vma2–GFP bound to vacuolar membranes in $rav1\Delta$ cells at 25 °C is 50% of that observed for wild-type cells (Fig. 5f). In contrast, co-immunoprecipitation and membrane-sedimentation experiments have shown that little or no intact V-ATPase complex is preserved in extracts of $rav1\Delta$ cells grown under the same conditions (Fig. 5b and data not shown). We speculate that RAVE promotes formation of stable V-ATPase by influencing the subunit composition or post-translational modification state of V_1. In the absence of RAVE, V_1 can bind to V_0 (albeit more slowly than when RAVE is present), but the assembled complex is less stable to perturbation, including *in vitro* manipulation. Further work will shed light on the detailed biochemical mechanism by which RAVE promotes V-ATPase assembly in resting cells and in cells that have been re-fed with glucose.

Methods

Yeast strains and growth media.

Tagged yeast strains were constructed as described[5]. *SKP1* and *CDC53* were modified with the tagging cassette pJS-M53H (ref. 5), whereas *RAV1*, *RAV2*, *RCY1* and *YBR280* were modified with a variant, pJS-TM53H (RDB1344), encoding nine copies of the Myc epitope preceded by the recognition site (ENLYFQG) for the tobacco etch virus (TEV)[28] protease. VMA2 and RAV1 were modified with pGFP53H (RDB1096), which encodes GFP. All knockout strains were created by oligonucleotide-mediated gene disruption[29], and were validated by PCR. Oligonucleotide sequences are available upon request. The following yeast strains were used: *CDC53–Myc₉* (RDY1250), *SKP1–Myc₉* (RDY1251), *RCY1–Myc₉* (RDY1510), *YBR280–Myc₉* (RDY1511), *RAV1–Myc₉* (RDY1512), *RAV2–Myc₉* (RDY1513), *rav1Δ* (RDY1645), *rav2Δ* (RDY1646), *RAV1–Myc₉ rav2Δ* (RDY1514), *RAV2–Myc₉rav1Δ* (RDY1515), *rav1Δ rav2Δ* (RDY1516), *SKP1–Myc₉ rav1Δ* (RDY1517), *SKP1–Myc₉ rav2Δ* (RDY1518), *VMA2–GFP* (RDY1519), *VMA2–GFP rav1Δ* (RDY1520), *RAV1–GFP* (RDY1647), *cdc53-1* (RDY690), *cdc34-2* (RDY670) and *skp1-12* (RDY1377).

For the experiments shown in Figs 1–3, unbuffered YP medium (pH ~6.5) was used. For the experiments shown in Figs 4, 5, YP medium was buffered to pH 5.5 with 50 mM MOPS plus 50 mM MES, or to pH 7.5 with 100 mM HEPES, as indicated.

Immunoprecipitation and mass spectrometry.

Epitope tagging of genes, preparation of cell extracts and immunoaffinity chromatography were carried out as described[5], except that immunoprecipitations and washes were carried out at pH 7.5 with 35 mg extract and 120 μl 9E10 beads. For the experiment shown in Fig. 2b, proteins were eluted with 0.1 mg ml⁻¹ TEV protease (GibcoBRL) at room temperature for 40 min. Eluted proteins were separated by one-dimensional SDS–PAGE, visualized by staining with silver, in-gel digested with trypsin and identified by mass spectrometry as described[30,31].

Active staining of vacuole with quinacrine.

Vacuolar acidification was measured by accumulation of fluorescent quinacrine[32]. Cells were grown in YP–dextrose (1% yeast extract, 2% peptone; ph 5.5) to an absorbance at 600 nm of 0.8–1.0, and 1 ml of the sample was collected and washed three times with uptake buffer (YP–dextrose, pH 7.5). The cell pellet was resuspended in 100 μl uptake buffer and quinacrine was added to a final concentration of 200 μM. Cells were then incubated for 10 min at 30 °C and were then kept on ice for 5 min, after which they were washed three times with ice-cold wash buffer (100 mM HEPES pH 7.5, and 2% glucose). Cell pellets were resuspended in 30 μl wash buffer and photographed within 1 h after quinacrine staining. To quantify quinacrine uptake, a culture grown in YP–dextrose (pH 5.5) was split into two, and the quinacrine fluorescence in 1 ml of cell suspension processed as described above was measured directly using a spectrofluorometer. The remainder of the cells were collected and weighed, and relative fluorescence was determined as total fluorescence per g of cells.

Membrane fractionation and native gel electrophoresis.

Wild-type and mutant cells were grown in YP–dextrose (pH 5.5) to an absorbance at 600 nm of 0.8–1.0 at 25 °C, or were transferred to YP–dextrose (pH 7.5) and further incubated at 33 °C for 1 h. Cells were then pelleted, washed once, resuspended in 1 ml of synthetic medium (buffered to pH 7.5 with 100 mM HEPES) containing 2% glucose and 1 M sorbitol, and spheroplasted by treatment with zymolase (0.1 units of zymolase per 10⁷ cells for 40 min at 30 °C with gentle shaking). For membrane fractionation, the resulting spheroplasts were quickly pelleted at 800g, resuspended in 1 ml ice-cold TE (10 mM Tris–HCl pH 7.5, and 1 mM EDTA), and lysed by rapid vortexing[31]. The suspension was centrifuged at 4 °C for 5 min at 800g to remove unlysed cells and the supernatant was centrifuged in a microfuge (14,000g at 4 °C for 10 min) to generate a crude membrane pellet. This pellet was washed once and resuspended in TE, pH 7.5.

For native gels, spheroplasts were pelleted and osmotically lysed on ice in native sample buffer (10 mM Tris acetate pH 6.9, 5 mM potassium acetate, 1 mM EDTA, 2 mM phenylmethylsulphonyl fluoride, 10% glycerol, 0.01% bromophenol blue and 0.01% xylene cyanol). Samples were then centrifuged to pellet particulate matter, and loaded immediately. Native gels[33] used a continuous buffer system of HEPES and imidazole at pH 7.4. Acrylamide gels (6%) were pre-run at a constant 120 V at 4 °C until the current was steady. Buffer was changed before loading of samples, and gels were run for 2 h at 120 V.

Microscopy and immunofluorescence.

For examination of Vma2–GFP and Rav1–GFP localization, cells grown in YP–dextrose (pH 5.5) at 30 °C were collected (for Rav1–GFP) or shifted to YP–dextrose (pH 7.5) at 37 °C for 1 h (for Vma2–GFP), and then resuspended in Vectashield mounting medium plus DAPI (Vector Laboratories) supplemented with 2% glucose. Cell suspensions were spotted onto microscope slides, allowed to settle for 5 min, and examined immediately with a ×100 objective (Fig. 5c, e).

For immunofluorescence, wild-type and *rav1Δ* cells grown in YP–dextrose (pH 5.5) at 25 °C to an absorbance at 600 nm of 0.8–1.0 were shifted to 37 °C for 1 h, fixed with 3.7% formaldehyde and hybridized with polyclonal anti-Vph1 antibody that was pre-absorbed with *vph1Δ* cell extract as described[33]. Cy3-conjugated anti-rabbit antibody was used at 1:1000 as a secondary antibody.

For analysis of V-ATPase reassembly, wild-type and *rav1Δ* cells expressing Vma2–GFP were treated as described[34]. At the indicated times, fixative (formaldehyde/glutaraldehyde to final concentrations of 3.7%/0.1%, respectively) was added directly to each culture, and cells were incubated for 30 min. Cells were then collected, resuspended in PBS plus 3.7% formaldehyde, and incubated for a further 6 h. Fixed cells were resuspended in Vectashield mounting medium, and observed using a Leica DM IRB/TCS confocal microscope.

1. Deshaies, R. J. SCF and Cullin/Ring H2-based ubiquitin ligases. *Annu. Rev. Cell Dev. Biol.* **15**, 435–467 (1999).
2. Tan, P. *et al.* Recruitment of a ROC1–CUL1 ubiquitin ligase by Skp1 and HOS to catalyze the ubiquitination of IκBα. *Mol. Cell* **3**, 527–533 (1999).
3. Ohta, T., Michel, J. J., Schottelius, A. J. & Xiong, Y. ROC1, a homolog of APC11, represents a family of cullin partners with an associated ubiquitin ligase activity. *Mol. Cell* **3**, 535–541 (1999).
4. Kamura, T. *et al.* Rbx1, a component of the VHL tumor suppressor complex and SCF ubiquitin ligase. *Science* **284**, 657–661 (1999).
5. Seol, J. H. *et al.* Cdc53/cullin and the essential Hrt1 RING-H2 subunit of SCF define a ubiquitin ligase module that activates the E2 enzyme Cdc34. *Genes Dev.* **13**, 1614–1626 (1999).
6. Skowyra, D., Craig, K. L., Tyers, M., Elledge, S. J. & Harper, J. W. F-box proteins are receptors that recruit phosphorylated substrates to the SCF ubiquitin-ligase complex. *Cell* **91**, 209–219 (1997).
7. Patton, E. E., Willems, A. R. & Tyers, M. Combinatorial control in ubiquitin-dependent proteolysis: don't Skp the F-box hypothesis. *Trends Genet.* **14**, 236–243 (1998).
8. Patton, E. E. *et al.* Cdc53 is a scaffold protein for multiple Cdc34/Skp1/F-box proteincomplexes that regulate cell division and methionine biosynthesis in yeast. *Genes Dev.* **12**, 692–705 (1998).
9. Bartel, P. L., Roecklein, J. A., SenGupta, D. & Fields, S. A protein linkage map of *Escherichia coli* bacteriophage T7. *Nature Genet.* **12**, 72–77 (1996).
10. Fromont-Racine, M., Rain, J. C. & Legrain, P. Toward a functional analysis of the yeast genome through exhaustive two-hybrid screens. *Nature Genet.* **16**, 277–282 (1997).
11. Stevens, T. H. & Forgac, M. Structure, function and regulation of the vacuolar (H⁺)-ATPase. *Annu. Rev. Cell Dev. Biol.* **13**, 779–808 (1997).
12. Forgac, M. Structure and properties of the vacuolar (H⁺)-ATPases. *J. Biol. Chem.* **274**, 12951–12954 (1999).
13. Parra, K. J. & Kane, P. M. Reversible association between the V1 and V0 domains of yeast vacuolar H⁺-ATPase is an unconventional glucose-induced effect. *Mol. Cell. Biol.* **18**, 7064–7074 (1998).
14. Zhang, J. W., Parra, K. J., Liu, J. & Kane, P. M. Characterization of a temperature-sensitive yeast vacuolar ATPase mutant with defects in actin distribution and bud morphology. *J. Biol. Chem.* **273**, 18470–18480 (1998).
15. Wiederkehr, A., Avaro, S., Prescianotto-Baschong, C., Haguenauer-Tsapis, R. & Riezman, H. The F-box protein Rcy1p is involved in endocytic membrane traffic and recycling out of an early endo-

some in *Saccharomyces cerevisiae*. *J. Cell. Biol.* **149**, 397–410 (2000).

16. Winzeler, E. A. *et al.* Functional characterization of the *S. cerevisiae* genome by gene deletion and parallel analysis. *Science* **285**, 901–906 (1999).

17. Spellman, P. T. *et al.* Comprehensive identification of cell cycle-regulated genes of the yeast *Saccharomyces cerevisiae* by microarray hybridization. *Mol. Biol. Cell* **9**, 3273–3297 (1998).

18. Uetz, P. *et al.* A comprehensive analysis of protein–protein interactions in *Saccharomyces cerevisiae*. *Nature* **403**, 623–627 (2000).

19. Marcotte, E. M. *et al.* Detecting protein function and protein–protein interactions from genome sequences. *Science* **285**, 751–753 (1999).

20. Kaplan, K. B., Hyman, A. A. & Sorger, P. K. Regulating the yeast kinetochore by ubiquitin-dependent degradation and Skp1p-mediated phosphorylation. *Cell* **91**, 491–500 (1997).

21. Galan, J. M. *et al.* Skp1p and the F-box protein Rcy1p form a non-SCF complex involved in recycling of the SNARE Snc1p in yeast. *Mol. Cell. Biol.* (in press).

22. Foury, F. The 31-kDa polypeptide is an essential subunit of the vacuolar ATPase in *Saccharomyces cerevisiae*. *J. Biol. Chem.* **265**, 18554–18560 (1990).

23. Weisman, L. S., Bacallao, R. & Wickner, W. Multiple methods of visualizing the yeast vacuole permit evaluation of its morphology and inheritance during the cell cycle. *J. Cell. Biol.* **105**, 1539–1547 (1987).

24. Manolson, M. F. *et al.* The VPH1 gene encodes a 95-kDa integral membrane polypeptide required for *in vivo* assembly and activity of the yeast vacuolar H($^+$)-ATPase. *J. Biol. Chem.* **267**, 14294–14303 (1992).

25. Rigaut, G. *et al.* A generic protein purification method for protein complex characterization and proteome exploration. *Nature Biotechnol.* **17**, 1030–1032 (1999).

26. Link, A. J. *et al.* Direct analysis of protein complexes using mass spectrometry. *Nature Biotechnol.* **17**, 676–682 (1999).

27. Verma, R. *et al.* Proteasomal proteomics: identification of nucleotide-sensitive proteasome-interacting proteins by mass spectrometric analysis of affinity-purified proteasomes. *Mol. Biol. Cell* **11**, 3425–3439 (2000).

28. Parks, T. D., Leuther, K. K., Howard, E. D., Johnston, S. A. & Dougherty, W. G. Release of proteins and peptides from fusion proteins using a recombinant plant virus proteinase. *Anal. Biochem.* **216**, 413–417 (1994).

29. Wach, A., Brachat, A., Pohlmann, R. & Philippsen, P. New heterologous modules for classical or PCR-based gene disruptions in *Saccharomyces cerevisiae*. *Yeast* **10**, 1793–1808 (1994).

30. Shevchenko, A., Wilm, M., Vorm, O. & Mann, M. Mass spectrometric sequencing of proteins silver-stained polyacrylamide gels. *Anal. Chem.* **68**, 850–858 (1996).

31. Shevchenko, A. *et al.* Linking genome and proteome by mass spectrometry: large-scale identification of yeast proteins from two dimensional gels. *Proc. Natl Acad. Sci. USA* **93**, 14440–14445 (1996).

32. Morano, K. A. & Klionsky, D. J. Differential effects of compartment deacidification on the targeting of membrane and soluble proteins to the vacuole in yeast. *J. Cell. Sci.* **107**, 2813–2824 (1994).

33. Tomashek, J. J., Sonnenburg, J. L., Artimovich, J. M. & Klionsky, D. J. Resolution of subunit interactions and cytoplasmic subcomplexes of the yeast vacuolar proton-translocating ATPase. *J. Biol. Chem.* **271**, 10397–10404 (1996).

34. Jackson, D. D. & Stevens, T. H. VMA12 encodes a yeast endoplasmic reticulum protein required for vacuolar H$^+$-ATPase assembly. *J. Biol. Chem.* **272**, 25928–25934 (1997).